Chemistry & Biology, Vol. 10, 491–502, June, 2003, ©2003 Elsevier Science Ltd. All rights reserved. DOI 10.1016/S1074-5521(03)00126-1

Rational Design of Alkylene-Linked Bis-Pyridiniumaldoximes as Improved Acetylcholinesterase Reactivators

Yuan-Ping Pang,[1,2,3,4,5,*] Thomas M. Kollmeyer,[1] Feng Hong,[1,6] Jong-Cheol Lee,[1] Pamela I. Hammond,[1] Sharie P. Haugabouk,[1] and Stephen Brimijoin[1,4]

[1]Department of Molecular Pharmacology and Experimental Therapeutics
[2]Mayo Clinic Cancer Center
[3]Tumor Biology Program
[4]Molecular Neuroscience Program
[5]Molecular Biophysics Program
Mayo Foundation for Medical Education and Research
200 First Street SW
Rochester, Minnesota 55905

Summary

To improve the potency of 2-pralidoxime (2-PAM) for treating organophosphate poisoning, we dimerized 2-PAM and its analogs according to Wilson's pioneering work and the 3D structure of human acetylcholinesterase (hAChE) inactivated by isoflurophate. 1,7-Heptylene-bis-*N,N'-syn*-2-pyridiniumaldoxime, the most potent of the alkylene-linked dimeric reactivators, was readily synthesized using bistriflate and is 100 times more potent than 2-PAM in reactivating hAChE poisoned by isoflurophate. Experimental and computational studies confirm that 2-PAM in its biologically active form adopts the *syn*-I configuration. Further, they suggest that the improved performance of dimeric oximes is conferred by two-site binding with one oxime pointing toward the diisopropyl ester at the catalytic site of hAChE and the other anchored at the peripheral site. This type of binding may induce a conformational change in the acyl pocket loop which modulates the catalytic site via a domino effect.

Introduction

Organophosphorous compounds have been used as chemical weapons (e.g., nerve agents such as sarin, soman, and VX) and as insecticides (e.g., chlorpyrifos, parathion, and coumaphos) [1]. Exposure to even small amounts of an organophosphorus compound can be fatal. The mechanism of organophosphate poisoning involves phosphorylation of a serine hydroxyl group in the active site of human acetylcholinesterase (hAChE), leading to inactivation of this essential enzyme. The therapeutic approach to organophosphate poisoning is to reactivate hAChE with a site-directed nucleophile. After reversibly binding to the active site, the nucleophile reacts with the phosphorylated hydroxyl group to release free, active enzyme while becoming phosphorylated itself in turn [2]. Drug design based on this chemical approach yielded 2-pralidoxime (2-PAM) and its analogs, which are effective antidotes for some organophosphates but not for others, such as soman [3, 4]. The variable performance is reportedly due to different rates of the irreversible dealkylation (aging) of various hAChE-organophosphate conjugates [5–8]. An additional reason for such variable performance is that the effect of an oxime depends on the equilibrium constant of Scheme I for a given organophosphate (Figure 2). Prior to aging, oximes are effective only when enzyme dephosphorylation is faster than oxime dephosphorylation. To improve 2-PAM, a clinical mainstay for treating organophosphate poisoning and yet a known alkylating agent, we made a series of dimeric oximes in pursuit of the following objectives: (1) increasing the affinity for the phosphorylated hAChE; (2) accelerating the rate of enzyme dephosphorylation; (3) reducing therapeutic dosage and therefore minimizing the nonspecific toxicity; and (4) gaining ability to counteract a wider range of organophosphates. These analogs were designed in light of the pioneering work of Wilson and Ginsburg and the 3D structure of diisopropylphosphoryl-hAChE, an immediate product of the reaction between isoflurophate and hAChE. The results described here help to explain why dimeric reactivators are more potent in reactivating hAChE than monomeric ones, and they provide insights into the design of further improved hAChE reactivators.

Results

Design

Inspired by the work of Wilson and Ginsburg [3, 9–14], we set out to synthesize dimeric analogs of 2-PAM that had not been reported in the literature. It was first necessary to decide whether the dimeric analogs adopt the *syn-I, syn-II*, or *anti* configuration (see Figure 1 for *syn* and *anti* definitions for oximes as well as the new nomenclature for oximes). Initially, *anti*-2-PAM was thought to be the biologically active and most stable configuration, into which *syn* stereoisomers convert slowly at room temperature (Figure 1) [15, 16]. Later, *syn*-I-2-PAM was suggested to be the biologically active and most stable configuration [17]. Recently, *syn*-II-2-PAM has been proposed to be the biologically active configuration [18]. This conflict in the literature prompted us to perform density functional theory calculations. Using the B3LYP/6-31+G(d,p)//B3LYP/6-31+G(d,p) method and the Onsager solvent model [19–22], we found that *syn*-I-2-PAM is ≈4 kcal/mol more stable than *anti*-2-PAM in vacuo or in water (Figure 1), and that *syn*-I-2-PAM is 0.6 and 1.0 kcal/mol more stable than *syn*-II-2-PAM in vacuo and in water, respectively (Figure 1). These results fit the experimental observation that crystalline 2-PAM adopts the *syn*-I configuration and are consistent with the reported proposal of *syn*-I-2-PAM being the biologically active and most stable configuration [17, 23]. It is therefore plausible that the biologically active form is *syn*-I

*Correspondence: pang@mayo.edu
[6]Current address: University of Washington, Department of Structural Biology, Box 357742, Seattle, Washington 98195.

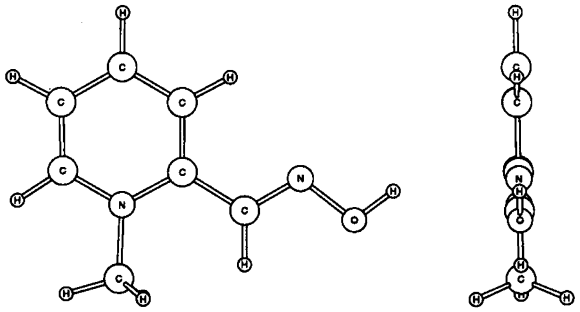

New nomenclature: (E)-s-trans
Old nomenclature: *syn* I

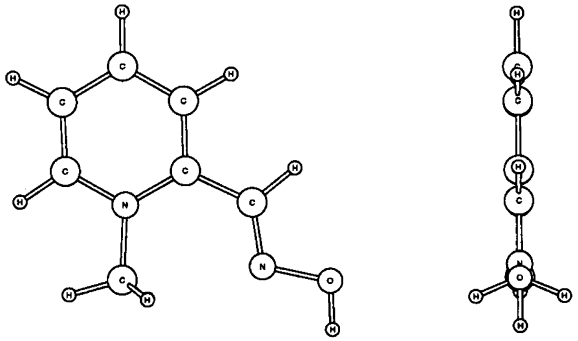

New nomenclature: (E)-s-cis
Old nomenclature: *syn* II

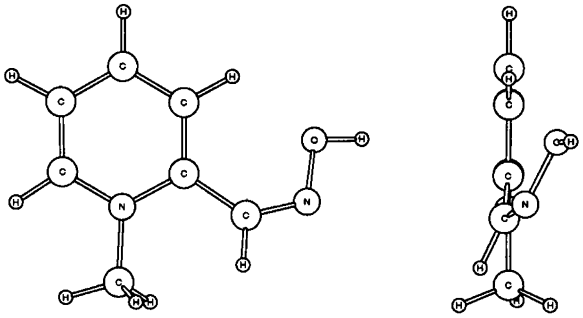

New nomenclature: Z
Old nomenclature: *anti*

configuration	E in vacuo (kcal/mol)	E in water (kcal/mol)
syn-I	-286460.9	-286462.3
syn-II	-286460.3	-286461.2
anti	-286456.8	-286458.3

Figure 1. The 3D Structures and Free Energies of 2-PAM in Three Energetically Stable Conformations Optimized by the DFT Calculations

Face view is shown on the left, side view is shown on the right, and E is the sum of electronic and thermal free energies.

and that *syn*-I-2-PAM should accordingly be used in the design of improved 2-PAM derivatives.

Viewed as pharmacophores to the active site of hAChE, pyridinium aldoximes are structurally analogous to 9-amino-1,2,3,4-tetrahydroacridine (THA), which binds, according to our previous work [24], to the catalytic and peripheral sites of hAChE (Figure 2). The expectation that these oximes bind to the same THA binding sites was confirmed by docking studies of 2-PAM and its analogs. We therefore hypothesized that the affinity for hAChE and the reactivation potency could be improved by tethering two oxime molecules with an alkyl chain spaced for simultaneous binding at the two THA binding sites. Two considerations support this hypothesis. First, the effective concentration of bis-oxime rises when one moiety anchors at the peripheral site and facilitates binding of the other moiety at the catalytic site because of the proximity effect (Figure 2). Elevating the effective concentration of dephosphorylated oxime shifts the chemical equilibrium toward the active enzyme, according to the principle of mass action (Scheme I of Figure 2). Second, the bis-oxime acquires a bulky phosphate group during enzyme reactivation and subsequently becomes too large to bind simultaneously at both catalytic and peripheral sites. The resulting fall in local concentration of phosphorylated oxime shifts the equilibrium further toward active hAChE. This hypothesis led to the synthesis of analogs **1e–h**, **2e–h**, and **3e–h** linked with alkyl chains (ω = 6, 7, 8, and 9) intended to bridge putative binding sites approximately 18 Å apart on hAChE, as reported previously (Figure 2) [24]. Short-chain analogs **1a–d** (ω = 2, 3, 4 and 5) and **3b–d** (ω = 3, 4 and 5) were also made and tested to ensure identification of the optimal length of linker. Analogs **1a–e** (ω = 2, 3, 4, 5 and 6), **1g** (ω = 8), **2b** (ω = 3), **2e** (ω = 6), and **3b–e** (ω = 3, 4, 5, and 6) were known in the literature [3, 9–14]. However, these compounds were synthesized in this study for biological testing and for improving synthetic yields, which were reportedly less than 7% for **3b–e**.

It might seem that introducing a superior ligand moiety such as THA [24] could more effectively increase the affinity of an aldoxime for hAChE. However, in the resulting structures, the high affinity moiety would compete for binding to the catalytic site, reduce oxime's access to the phosphonyl group of the enzyme, and impede reactivation. Introducing a high affinity peripheral-site ligand (e.g., propidium [25]) would cause different problems: strong binding and persistent inhibition regardless of phosphorylation. For these reasons, we confined our investigation to homodimeric reactivators.

Synthesis

Compounds **1b–h** and **2e–h** were readily synthesized in good yields by quaternization of 3- or 4-pyridinealdoxime with dibromoalkanes using the method by Poziomek et al. [9]. Compound **1a** was prepared in a higher yield by our modified procedure using a Parr reaction vessel. However, the dibromoalkane protocol was problematic for compound **3**. Low yields (< 7%) were obtained, probably due to steric hindrance of pyridine nitrogen by the 2-*syn*-pyridinealdoxime [3, 15]. We unsuccessfully attempted to couple two 2-pyridinealdehydes with dibromoalkane and then convert the aldehydes to oximes in DMSO or aqueous media. Subsequently, by using

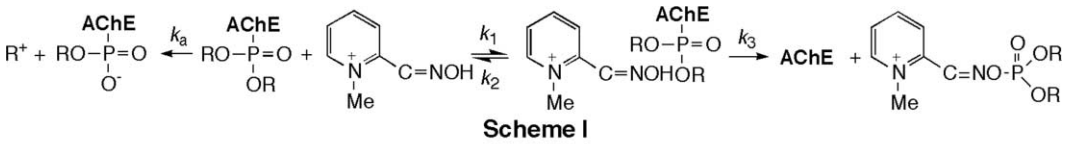

Scheme I

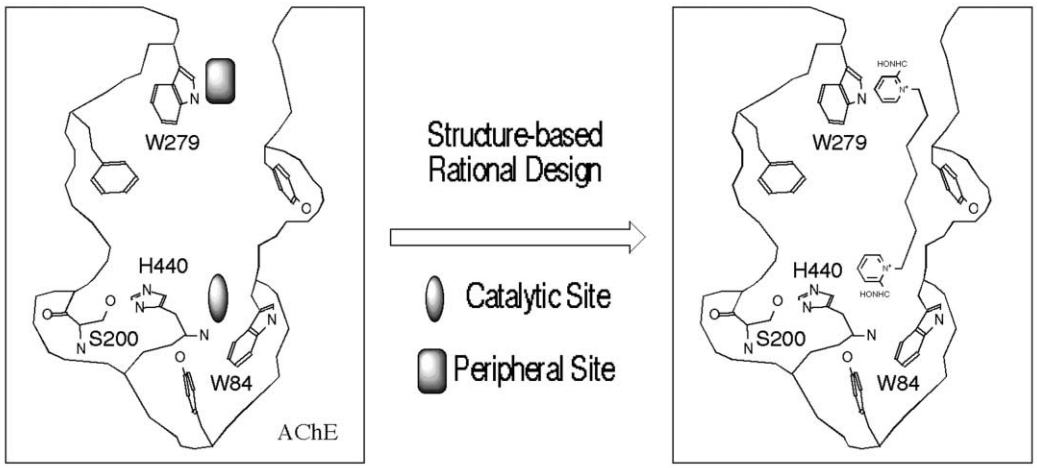

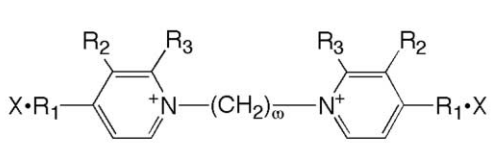

1: R_1 = CHNOH, R_2 = H, R_3 = H, X = Br^-;
2: R_1 = H, R_2 = CHNOH, R_3 = H, X = Br^-;
3: R_1 = H, R_2 = H, R_3 = CHNOH, X = Cl^-.
a: ω = 2; b: ω = 3; c: ω = 4; d: ω = 5;
e: ω = 6; f: ω = 7; g: ω = 8; h: ω = 9.

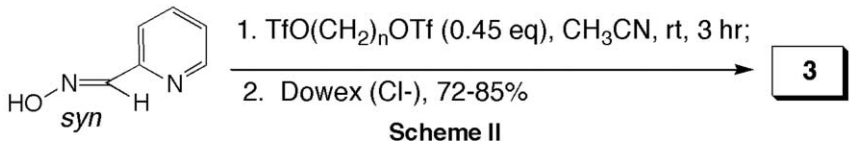

Scheme II

Figure 2. The Reactivation Mechanism and the Design and Synthesis of Dimeric Oximes

bistriflates [26, 27] as alkylating reagents in CH_3CN at room temperature, we succeeded in coupling two *syn*-2-pyridinealdoximes. The resulting triflate salts were subjected to ion-exchange chromatography on Dowex-Cl^- resins, yielding **3b–h** in high yields (72%–85%) on gram scale (Scheme II of Figure 2). This method represents greater than a 10-fold improvement in yield compared to previously reported methods [3, 15]. However, quaternization of *syn*-2-pyridinealdoximes with ethylene-bistriflate failed to yield **3a**.

Testing

For in vitro reactivation screening, hAChE from red blood cells was inhibited by the organophosphate drug, echothiophate, followed by treatment with 1.0 μM reactivator for 60 min (see Experimental Procedures). Under these conditions, 2-PAM led to modest reactivation (6%), and **2e–h** were only slightly more effective (7%–19%). By contrast, **1e–h** and **3e–h** were markedly more effective (reactivation up to 52% and 99%, respectively).

Reactivation was expected to depend on linker chain length (Figure 3). To make certain of discovering optimal compounds, a wide range of lengths was tested in series **1** and **3**. Shorter chain analogs of **2** were not produced, since **2e–h** were only slightly better than 2-PAM, and 3-methylpyridiniumaldoxime was less effective than 2-PAM or 4-methylpyridiniumaldoxime (4-PAM) [16]. In the screening assay, the most effective of the 4-pyridiniumaldoxime reactivators were the shortest, **1a** and **1b**, yielding ≈50% reactivation when tested at a concentration of 1 μM. Under the same conditions, however, **3e** with a hexylene chain and **3f** with a heptylene chain demonstrated 89 ± 3.7% and 99 ± 3.9% reactivations, respectively ($n = 7$). Although the difference in reactivation potency between **3e** and **3f** was not significant by simple t test, reactivation by **3f** in each experiment averaged 10% greater than that by **3e** ($p < 0.01$). Analogs with longer and shorter linkers were substantially less effective. Thus, the most effective reactivator in our series was a heptylene-linked bis-oxime.

Further experiments were performed to determine the kinetics of reactivation, since enzyme activity measured at one time and concentration does not define inherent potential. Kinetic constants for reactivation by 2-PAM,

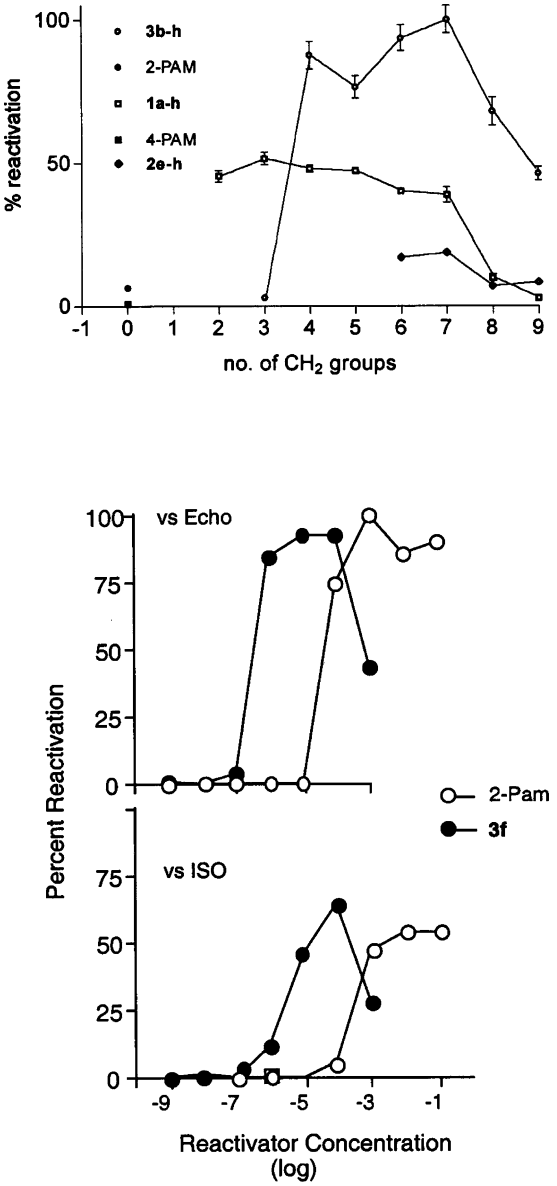

Figure 3. Reactivation of the Poisoned hAChE by Oximes and Their Dimeric Analogs

The top shows reactivation activities of the echothiophate-poisoned AChE by 2- and 4-PAM and their dimeric analogs linked with different numbers of methylene groups. All agents were tested at a concentration of 10^{-6} M and an exposure time of 60 min. The bottom shows dose-response curves demonstrated by **3f** or 2-PAM in reactivating AChE poisoned by echothiophate (Echo) or isoflurophate (ISO).

4-PAM, and bis-oximes were derived from the time course of hAChE recovery in the presence of varying concentrations of oxime (see Experimental Procedures). With echothiophate-treated hAChE, reactivation rates depended on oxime structure and concentration (Figure 3) and were well described by theoretical curves based on the presumed reaction scheme.

The reactivation rate constants (k_3) for all oximes studied (Table 1) showed that **1b** was the fastest reactivator, with a k_3 of 1.2 min^{-1}. As the alkylene linkage in this series lengthened, the rate constant steadily decreased by 3 orders of magnitude, to a value of 0.0026 min^{-1} for **1h**. Values from series **3** followed an inverted U-curve: k_3 first increased to a peak at 0.12 min^{-1} with **3c**, then declined to a minimum of 0.023 min^{-1} with **3h**.

Affinity for hAChE was measured in two ways. First, an estimate of oxime affinity for the free enzyme was obtained by determining K_i values for hAChE inhibition in standard experiments on substrate kinetics (Table 1). By this measure, compounds **3b–g** were generally about 3-fold more potent inhibitors than their counterparts, **1b–g**. In both series, K_i decreased by roughly 2-fold with each methylene addition. However, a 10-fold decrease was seen at the change from 5 to 6 methylene groups in **3d** to **3e**.

In order to determine oxime affinity for phosphorylated enzyme, K_D values were extracted from the data on reactivation as a function of time and oxime concentration (see Biological Testing under Experimental Procedures). For most compounds, K_D was less than or equal to K_i, and, like K_i, it decreased with increasing linker length. This effect was more pronounced with series **1** (300-fold change from **1b** to **1h**) than with series **3** (35-fold change from **3b** to **3h**). In series **3**, moving from **3d** to **3e**, K_D did not show the large drop that was seen in K_i, but it did drop markedly in series **1**, moving from **1f** to **1g**.

The overall efficiency for reactivation of hAChE is described by the ratio k_3/K_D. By this definition, the most effective reactivator optimally combines rapid action and high affinity for the phosphorylated hAChE. Because k_3/K_D in the bisoximes is maximal for **3f**, this agent was compared further with 2-PAM in order to determine relative potency in reactivating hAChE after inhibition with echothiophate and also isoflurophate. Although isoflurophate-treated hAChE did not reactivate as readily as echothiophate-treated hAChE, full dose-response curves demonstrated that **3f** was 100 times more effective than 2-PAM in reactivating hAChE poisoned by either organophosphate (Figure 3).

Modeling of Diisopropylphosphoryl-hAChE

It is difficult to experimentally determine the 3D structure of diisopropylphosphoryl-hAChE because dealkylation of the diisopropylphosphoryl group (referred to as "aging" of the phosphorylated hAChE) occurs so quickly. However, this structure is accessible computationally through a systematic conformational search of the diisopropylphosphoryl group attached to Ser200 followed by energy minimization and multiple molecular dynamics (MD) simulations [28–31]. In the modeling of the phosphorylated hAChE, the common "loop-in" formation (the side chain of Arg289 pointing outward, Figure 4) of the acyl pocket loop (residues 278–292, based on the *Torpedo* numbering) was used in the hope that the diisopropylphosphoryl group may induce the "loop-out" conformation (the side chain of Arg289 pointing inward, Figure 4) of the acyl pocket loop found uniquely in the crystal structure of an aged phosphylated AChE (PDB ID code 2DFP) [32], if indeed the loop-out conformation is energetically more stable than the loop-in conformation. Despite the enhanced sampling achieved by performing 20 independent 1.0 ns (1.0 fs time step) MD

Table 1. Kinetic Constants for Oxime Reactivators

Compound	n*	K_i (μM)	K_D (μM)	k_3 (min^{-1})	k_3/K_D*1000
4-PAM	0	580	733	0.055	0.1
1a	2	270	62	0.700	11
1b	3	170	66	1.200	18
1c	4	57	75	0.740	10
1d	5	35	20	0.440	23
1e	6	11	10	0.185	18
1f	7	3.3	4.3	0.056	13
1g	8	2.1	0.3	0.005	20
1h	9	1.3	0.2	0.002	12
2-PAM	0	470	250	0.330	1.3
3b	3	65	21	0.048	2.3
3c	4	32	15	0.120	7.6
3d	5	21	6.9	0.091	13
3e	6	2.2	2.4	0.120	51
3f	7	1.3	1.4	0.120	85
3g	8	0.6	0.5	0.034	66
3h	9	0.3	0.6	0.023	37

* = number of methylene groups used to tether two pyridiniumaldoximes.

simulations of the phosphorylated hAChE with different initial velocities [28–31], no conversion to the loop-out conformation was observed in any of these simulations. It would be interesting to compare the average potential energy of the "apo" phosphorylated hAChE adopting the loop-in conformation in water with that of the loop-out conformation. However, due to the limitation of our computing resources, we did the comparative energetics studies using the hAChE complexes instead of the apo enzyme (vide infra). In the most energetically stable diisopropylphosphoryl-hAChE structure with the loop-in conformation refined by multiple MD simulations, the double-bond oxygen atom of the phosphate group rests in the oxyanion hole of the active site of hAChE. That result is consistent with the assignment of this oxygen atom to the oxyanion hole in five crystal structures of phosphorylated AChE (PDB ID codes 1CFJ, 1SOM, 1VXO, 1VXR, and 2DFP) [32, 33]. The two isopropyl groups interact favorably with Trp84, Gly119, Tyr121, Trp233, Phe288, Phe290, Tyr330, and Phe331. Interestingly, His440 forms two hydrogen bonds with Glu199 and Glu327, instead of forming two hydrogen bonds with Glu327 and the phosphate, as seen in the crystal structures of dealkylated (aged) phosphorylated AChE (PDB ID codes 1CFJ, 1SOM, 1VXO, and 2DFP), or forming two hydrogen bonds with Glu199 and a water molecule, as seen in the crystal structure of phosphorylated AChE (PDB ID code 1VXR) [32, 33]. However, the unique hydrogen bond pattern of His440 in the diisopropylphosphoryl-hAChE structure predicted by computer modeling is akin to the report that His440 is mobile in the active site of hAChE [33].

Modeling of Diisopropylphosphoryl-hAChE-3f

The EUDOC-generated diisopropylphosphoryl-hAChE-**3f** structure with the loop-in conformation was refined by ten independent 1.0 ns (1.0 fs time step) MD simulations with different initial velocities. No conversion to the loop-out conformation was observed in any of these simulations, despite the fact that the active site of hAChE was occupied, in this case, by two bulky groups of the diisopropylphosphoryl ester and **3f**. A new set of ten simulations was then carried out with the same diisopropylphosphoryl-hAChE-**3f** structure, except that the loop-in conformation was manually changed to the loop-out conformation according to the crystal structure of

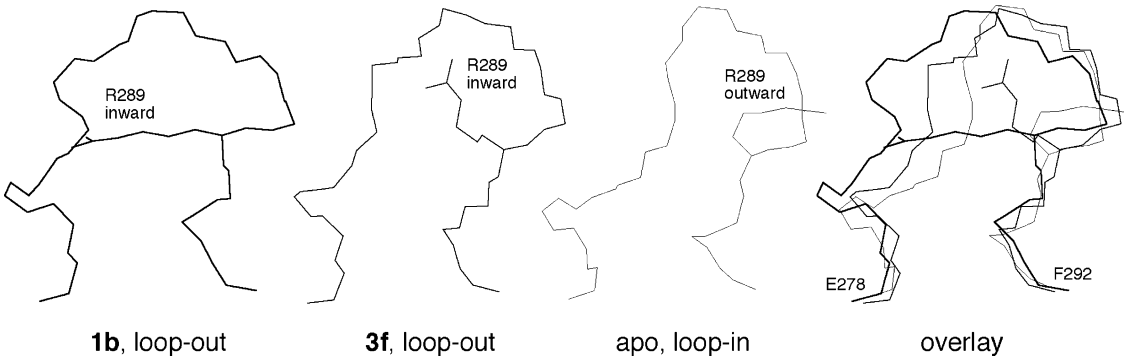

Figure 4. The Effects of the Binding of **1b** and **3f** on the Backbone Conformation of the Acyl Pocket Loop in Diisopropylphosphoryl-hAChE

Apo, diisopropylphosphoryl-hAChE; **3f**, diisopropylphosphoryl-hAChE bound with **3f**; **1b**, diisopropylphosphoryl-hAChE bound with **1b**; and overlay, an overlay of the three conformations showing that the loop is pushed out further when the diisopropyl ester is lifted in the **1b** complex.

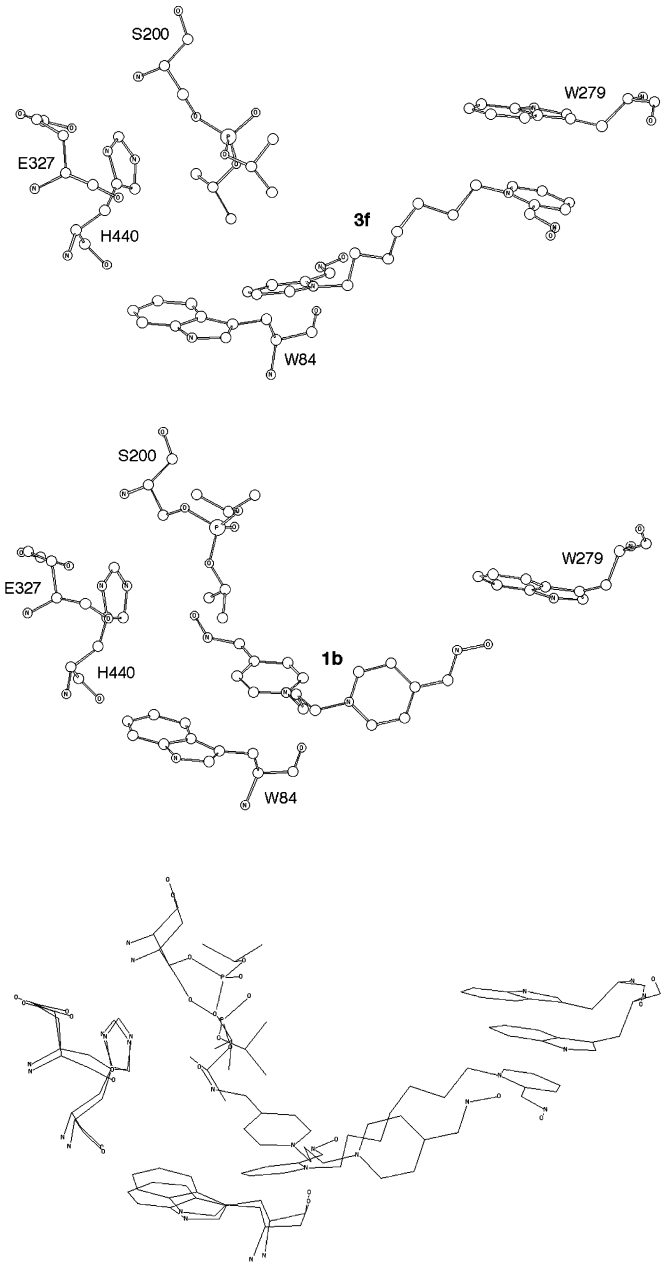

Figure 5. Close-Up Views of the Binding of **1b** and **3f** in Diisopropylphosphoryl-hAChE

The top shows binding with **3f**, the middle shows binding with **1b**, and the bottom shows an overlay of the two complexes demonstrating that the diisopropyl ester is lifted in the **1b** complex.

an aged phosphylated hAChE (PDB ID code 2DFP) [32]. In the second set of simulations, no conversion to the loop-in conformation was observed either. However, the average potential energy of the most energetically stable protein complex structure adopting the loop-out conformation in water simulation is 22.1 kcal/mol lower than the corresponding one adopting the loop-in conformation. This energy difference suggests that the loop-out conformation is preferred for the acyl pocket loop in the diisopropylphosphoryl-hAChE-**3f** complex and that more simulations with longer time frames are required to observe the exchange of the two loop conformations. In the most energetically stable Michaelis-Menten complex of diisopropylphosphoryl-hAChE-**3f** with the loop-out conformation (Figure 5), the pyridinium group at the peripheral site interacts with Tyr70, Tyr121, and Trp279 via cation-pi interactions and electrostatically with Asp72; the oxime oxygen atom forms a hydrogen bond with a water molecule; the pyridinium group at the catalytic site interacts with Trp84, Tyr330, and Tyr334 via cation-pi interactions and electrostatically with Asp72 and Glu199; the oxime oxygen atom at the catalytic site forms a hydrogen bond with a structural water molecule that is a part of the hydrogen bond network consisting of Tyr130, Glu199, Tyr330, and five structural water molecules at the catalytic site; one isopropyl group has van der Waals interactions with the alkylene chain of **3f**; and the distance of the oxime oxygen atom to the phosphorus atom is 7.2 Å, while the distance between the two oxime-oxygen atoms is 13.0 Å.

Modeling of Diisopropylphosphoryl-hAChE-1b

The average potential energy of the most energetically stable **1b** complex structure adopting the loop-out con-

formation in water is 1.0 kcal/mol lower than the corresponding one adopting the loop-in conformation. This small energy difference was confirmed by 20 additional independent 2.0 ns (1.0 fs time step) MD simulations with different initial velocities (ten for the loop-in and ten for the loop-out). Likewise, in the most energetically stable Michaelis-Menten complex of diisopropylphosphoryl-hAChE-**1b** with the loop-out conformation (Figure 5), one pyridinium group interacts with Tyr70, Tyr72, Tyr334, and Asp72; the other pyridinium group interacts with Trp84, Glu199, and Asp72; one hydroxyl hydrogen atom forms an aromatic hydrogen bond with the aromatic ring of Trp279 [34]; the other oxime group has a hydrogen bond with Glu199 and points toward the phosphoric acid diisopropyl ester; one isopropyl group has van der Waals interactions with the alkylene chain of **1b**; and the distance between the phosphorus atom and the oxime oxygen atom is 6.5 Å, while the distance between the two oxime-oxygen atoms is 14.7 Å. Interestingly, because of the hydrogen bond of the oxime group with Glu199, the pyridinium group goes underneath the diisopropyl ester by lifting the ester and, in turn, pushes the acyl pocket loop further out relative to the acyl pocket loop of diisopropylphosphoryl-hAChE-**3f** (Figure 4). Another difference compared to the complex with **3f** is that the hydrogen bond network at the catalytic site in the **1b** complex is comprised of Tyr130, Glu199, Tyr330, and three structural water molecules.

Discussion

Biologically Active Configuration of 2-PAM

While in vivo studies are underway to evaluate **3f** as a potential antidote for organophosphate poisoning, the present work helps to understand why dimeric oximes are more potent than the monomeric oximes and provides insights into rational design of further improved hAChE reactivators. A key insight relates to oxime conformation. Contradictory to the early reports [15–17], *syn*-II-2-PAM (E-*syn*-2-PAM, Figure 1) has recently been proposed to be the biologically active form [18]. This proposal was based on the finding that the reactivation activity of a 2-PAM analog constrained in the E-*syn* conformation was comparable to that of 2-PAM itself [18]. Without knowing the relative energies of 2-PAM in its different conformations and their interaction energies with the inactivated hAChE, it is difficult to determine whether 2-PAM adopts the *syn*-I or *syn*-II conformation in its biologically active form. According to our density functional theory calculations, *syn*-I-2-PAM is 0.6 and 1.0 kcal/mol more stable than *syn*-II-2-PAM in vacuo and in water, respectively (Figure 1). These results imply that the interaction energy of *syn*-II-2-PAM with the inactivated hAChE ought to be 0.6 kcal/mol lower than that of *syn*-I-2-PAM for 2-PAM to adopt the *syn*-II conformation in the active site of diisopropylphosphoryl-hAChE. On the contrary, the docking studies reveal that the calculated interaction energy of *syn*-II-2-PAM is 0.8 kcal/mol higher than that of *syn*-I-2-PAM (Table 2). In addition, the 2-pyridiniumaldoxime group of **3f** in the most energetically stable complex of diisopropylphosphoryl-hAChE-**3f** also adopts the *syn*-I configuration. Altogether, the *syn*-I configuration previously reported as the biologically active configuration [17] should be used in the design of further improved 2-PAM analogs as hAChE reactivators.

Structure-Activity Relationship

Both series **1** (*para*-oxime) and series **3** (*ortho*-oxime) demonstrated the dependency of reactivation potency upon linker chain length (Figure 3). However, the fastest and more effective reactivator for the para series is the dimer linked with three methylene groups (**1b**), whereas the most effective one for the ortho series is linked with seven methylene groups (**3f**). The 3D structures of complexes **1b** and **3f** can explain the different requirements of linker chain length for reactivation improved by two-site binding. In the 3D structures, **1b** and **3f** span the active site of the phosphorylated hAChE; and the distances between the two oxime-oxygen atoms as nucleophiles in **1b** and in **3f** are 14.7 Å and 13.0 Å, respectively, even though **1b** is tethered by a short chain. It is therefore conceivable that short linkers are required for the more effective *para*-bisoximes and that long linkers are required for the more effective *ortho*-bisoximes.

As early as the 1950s, some compounds **1** (ω = **1**, 2, 3, 4, 5, 6, 8, and 10), **2** (ω = 3 and 6), and **3** (ω = 3, 4, 5, and 6) had been made and reported collectively by a number of independent groups [3, 9–14]. However, the explanation of why the dimeric analogs are more potent in reactivating hAChE than the monomeric ones was not satisfactory, nor was it fully understood why 2-PAM is more potent than 4-PAM, especially since the assumption that 2-PAM adopts the *anti* configuration [16] must be abandoned. In the present study, we have found that the calculated interaction energy of a reactivator tends to be inversely related to the reactivation potency (Table 2). The finding supports the design principle described above: reactivators with increased affinity for the active site of the phosphorylated hAChE accelerate the rate of enzyme dephosphorylation (Scheme I of Figure 2). It is evident from the decomposed interaction energies in Table 2 that the binding of oxime derivatives to the inactivated hAChE is driven mainly by the electrostatic interactions between the cationic oximes and the electron-rich binding region of the enzyme. This explains, at the atomic resolution, the experimental observation that the neutral 2-pyridinealdoxime is far less efficient than the cationic 2-PAM in reactivating hAChE [16]. The data in Table 2 also indicate that 2-PAM is more potent in reactivating hAChE than 4-PAM, because 2-PAM better fits the active site of the poisoned hAChE than 4-PAM both sterically and electrostatically. An additional reason is that the phosphorylated 4-PAM that is generated after enzyme reactivation has a half-life (980 s) 100 times longer than that of the phosphorylated 2-PAM (10 s), and the subsequent inhibition of hAChE by the phosphorylated 4-PAM makes 4-PAM less effective in reactivating the phosphorylated hAChE than 2-PAM [37]. Furthermore, the nearly doubled interaction energies of the dimeric oximes relative to those of the monomeric ones in Table 2 indicate that the two-site binding of the dimeric oximes markedly lowers the interaction energies (increases the binding affinities). These structural insights explain why dimeric reactivators are more potent than the monomeric ones.

Table 2. Interaction Energies of Oximes with Diisopropylphosphoryl-hAChE

	Eint (kcal/mol)				Eout-Ein
Reactivator	vdw	ele	total	k_3/K_D*1000	(kcal/mol)
3f	−49.7	−307.1	−356.8	85	−22.1
1b	−41.4	−312.5	−353.9	18	−1.0
syn-I-2-PAM	−25.9	−140.2	−166.1	1.3	−256.6
syn-II-2-PAM	−21.8	−143.5	−165.3	N/A	−248.4
syn-I-4-PAM	−22.7	−123.9	−146.6	0.1	−233.2

Calculated energies with enzyme adopting the loop-out conformation (Eout) are shown along with experimentally determined kinetic constants of diisopropylphosphoryl-hAChE complexed with oximes (k_3/K_D). Differences in the average potential energy of the hAChE complex between the loop-out and loop-in conformations of the acyl pocket loop are also given (Eout-Ein).

Domino Effect

One would need an investigation of the conformational stability of the "apo" phosphorylated hAChE adopting the loop-out conformation to determine whether the unaged hAChE poisoned by isoflurophate adopts the loop-out conformation like the aged phosphylated *Torpedo* AChE [32]. However, our modeling of loop-in and loop-out conformations in the hAChE complexes does suggest that the loop-out conformation is preferred in diisopropylphosphoryl-hAChE. This preference is strengthened when diisopropylphosphoryl-hAChE is complexed with monomeric oximes, because much larger differences in average potential energy of the hAChE complex (233.2 to 256.6 kcal/mol) were found between the two loop conformations (Table 2). Although the acyl pocket loop is relatively distal to the bound reactivators, overlay of the two computer-generated **1b** and **3f** complexes reveals significant conformational changes of the acyl pocket loop and of the diisopropylphosphoryl ester (Figure 5). These changes are apparently caused by the binding of different reactivators via a domino effect involving the acyl pocket loop, the diisopropylphosphoryl ester, and the bound reactivator. This domino effect is important to rational design of hAChE reactivators in that it calls for the attention to the modulation of the active site by the relatively distal, species-specific actyl pocket loop. On the one hand, our computationally exhaustive multiple MD simulation studies with an equivalent of 250,000 hr of CPU time of the 2.2 Ghz Xeon P4 processor failed to generate the loop-out conformation a priori, which underscores the crucial role of the insightful X-ray structure adopting the loop-out conformation in rational design of hAChE reactivors. On the other hand, the recently reported AChE species specificity demonstrated by reversible and pseudo-irreversible AChE inhibitors [38, 39] would discourage the direct use of the X-ray structures of *Torpedo* AChE in the design of hAChE reactivators, especially given the fact that the amino acid sequence of the acyl pocket loop is not conserved between human and *Torpedo* enzymes. A combination of the experimental and computational approaches is suggested here to address the domino effect on each designed hAChE reactivator.

Reactivators of the Aged hAChE

Following on the present work, still better hAChE reactivators might be crafted by docking various oxime derivatives in consideration of the domino effect, synthesizing those with interaction energies lower than that of bis-7-*syn*-I-2-PAM, and testing them experimentally. In our opinion, further development of hAChE reactivators should be directed toward finding novel nucleophiles that are capable of dephosphorylating the dealkylated phosphoryl hAChE, i.e., aged hAChE. The search can be facilitated by the concepts illustrated here, dimerization of low-affinity nucleophiles and theoretical estimation of interaction energies, before launching into synthesis and testing.

Significance

Employing the bivalence approach, we have developed 1,7-heptylene-bis-*N,N'*-*syn*-2-pyridiniumaldoxime dichloride. This hAChE reactivator can be readily synthesized by using bistriflate and is a promising antidote with less liability to induce chronic toxicity caused by alkylation or other nonspecific means, as it is 100 times more potent than 2-PAM in reactivating hAChE after exposure to echothiophate or isoflurophate. Our study suggests the use of *syn*-I-2-PAM in rational design of 2-PAM analogs as improved hAChE reactivators. Our results also indicate that novel hAChE reactivators can be developed by dimerizing appropriate nucleophiles while taking into account the modulation of the active site by the relatively distal actyl pocket loop via the domino effect involving the acyl pocket loop, the alkylphosphoryl ester, and the bound reactivator. This kind of approach may ultimately result in reactivators capable of dephosphorylating the aged hAChE.

Experimental Procedures

Syn-pyridine-2-aldoxime, pyridine-3-aldoxime, pyridine-4-aldoxime, 1,3-dibromopropane, 1,4-dibromobutane, 1,6-dibromohexane, 1,7-dibromoheptane, 1,8-dibromooctane, and 1,9-dibromononane were purchased from Aldrich Chemical Company (Milwaukee, WI) and were used without further purification. 1,2-dibromoethane and 1,5-dibromopentane were purchased from Acros Organics USA (Morris Plains, NJ) and were used without further purification. Methyl *t*-butylether (MTBE), methylene chloride, ethyl acetate, and acetonitrile were purchased from Fisher Scientific Company, L.L.C. (Pittsburgh, PA) and used as received, except for methylene chloride that was distilled from calcium hydride before use. Pyridine-2-aldoxime methochloride was purchased from Sigma (St. Louis, MO). Bistriflates were prepared in accordance with a published procedure [26]. All reactions were performed under N_2 with stirring. Elemental analyses were performed by either Quantitative Technologies Incorporated or Atlantic Microlabs Incorporated on recrystallized sam-

ples after lypholization from 0.5 ml of water. The recrystallization using water was carried out to remove residual methanol resulted from the previous crystallization using methanol/ether. NMR spectra were obtained on Bruker AC-300, Bruker Avance 500, or Bruker Avance 600 instruments. Chemical shifts are reported in δ units using TMS (δ = 0 ppm) as an internal standard for ^{1}H-NMR spectra. ^{13}C-NMR spectra are referenced to solvent peak when dissolved in DMSO-d_6 and referenced to $CDCl_3$ (δ = 77.0 ppm) as an external standard when dissolved in D_2O. Coupling constants are reported in Hertz. All bis-oxime products decomposed (>175°C) before melting.

1,2-Ethylene-bis-*N,N'*-4-Pyridiniumaldoxime Dibromide (1a)
Pyridinium-2-carboxaldehyde oxime (1.00 g, 8.2 mmol), 1,2-ethylene dibromide (0.28 ml, 3.2 mmol), and absolute ethanol (10 ml) were added to a 23 ml Parr reaction vessel. The vessel was sealed, then placed in a 130°C oven for 48 hr. After cooling to room temperature, the Parr reaction vessel was opened and the reaction mixture was filtered. The precipitate was added to water (100 ml) and extracted with ethyl acetate (3 × 50 ml). The aqueous solution was lyophilized to give a crude product that was recrystallized from a mixture of water (20 ml) and isopropanol (50 ml). Yield: 63% as white powder; ^{1}H-NMR (300 MHz, DMSO-d_6) δ 12.87 (s, 2 H), 8.88 (d, 4 H, J = 6.8 Hz), 8.45 (s, 2 H), 8.27 (d, 4 H, J = 6.7 Hz), 5.21 (s, 4 H); ^{13}C-NMR (75.46 MHz, D_2O) δ 153.1, 148.6, 147.4, 128.1, 62.2. Anal. ($C_{14}H_{16}Br_2N_4O_2 \cdot 1.1H_2O$) C, H, N.

The general procedure for synthesis of **1b–h** and **2e–h** was as follows: 4-Pyridinealdoxime (2.8 g, 23.4 mmol) and 1,7-dibromoheptane (2.0 g, 7.8 mmol) were added to 30 ml of absolute ethanol. The reaction mixture was heated at reflux for 48 hr and then cooled to room temperature. The product was collected by filtration, rinsed with 2 ml of cold absolute ethanol, then dried under vacuum.

1,3-Propylene-bis-*N,N'*-4-Pyridiniumaldoxime Dibromide (1b)
Yield: 79% as white powder; ^{1}H-NMR (300 MHz, DMSO-d_6) δ 12.86 (s, 2H), 9.07 (d, 4 H, *J* = 6.8 Hz), 8.46 (s, 2 H), 8.28 (d, 4 H, *J* = 6.7 Hz), 4.71 (t, 4 H, *J* = 7.3 Hz), 2.64 (p, 2 H, *J* = 7.2 Hz); ^{13}C-NMR (75.46 MHz, D_2O) δ 151.6, 148.8, 147.3, 127.8, 60.4, 34.4. Anal. ($C_{15}H_{18}Br_2N_4O_2 \cdot H_2O$) C, H, N.

1,4-Butylene-bis-*N,N'*-4-Pyridiniumaldoxime Dibromide (1c)
Yield: 93% as white powder; ^{1}H-NMR (300 MHz, DMSO-d_6) δ 12.84 (s, 2 H), 9.04 (d, 4 H, *J* = 6.8 Hz), 8.44 (s, 2 H), 8.25 (d, 4 H, *J* = 6.7 Hz), 4.63 (m, 4 H), 1.95 (m, 4 H); ^{13}C-NMR (75.46 MHz, D_2O) δ 151.3, 148.7, 147.1, 127.6, 63.1, 29.9. Anal. ($C_{16}H_{20}Br_2N_4O_2$) C, H, N.

1,5-Pentylene-bis-*N,N'*-4-Pyridiniumaldoxime Dibromide (1d)
Yield: 73% as white powder; ^{1}H-NMR (300 MHz, DMSO-d_6) δ 12.83 (s, 2 H), 9.10 (d, 4 H, *J* = 6.6 Hz), 8.45 (s, 2 H), 8.25 (d, 4 H, *J* = 6.7 Hz), 4.60 (t, 4 H, *J* = 7.3 Hz), 1.97 (m, 4 H), 1.32 (p, 2 H, *J* = 6.8 Hz); ^{13}C-NMR (75.46 MHz, D_2O) δ 150.9, 148.7, 147.2, 127.5, 63.7, 32.6, 24.7. Anal. ($C_{17}H_{22}Br_2N_4O_2 \cdot 0.3\ H_2O$) C, H, N.

1,6-Hexylene-bis-*N,N'*-4-Pyridiniumaldoxime Dibromide (1e)
Yield: 87% as white powder; ^{1}H NMR (300 MHz, DMSO-d_6) δ 12.83 (s, 2 H), 9.04 (d, 4 H, *J* = 6.6 Hz), 8.44 (s, 2 H), 8.24 (d, 4 H, *J* = 6.7 Hz), 4.56 (t, 4 H, *J* = 7.4 Hz), 1.94-1.87 (m, 4 H), 1.35-1.30 (m, 4 H); ^{13}C NMR (75.46 MHz, DMSO-d_6) δ 148.3, 145.1, 145.0, 124.0, 60.0, 30.2, 24.6. Anal. ($C_{18}H_{24}Br_2N_4O_2$) C, H, N.

1,7-Heptylene-bis-*N,N'*-4-Pyridiniumaldoxime Dibromide (1f)
Yield: 85% as white needles; ^{1}H-NMR (300 MHz, DMSO-d_6) δ 12.83 (s, 2 H), 9.04 (d, 4 H, *J* = 6.3 Hz), 8.44 (s, 2 H), 8.24 (d, 4 H, *J* = 6.6 Hz), 4.56 (t, 4 H, *J* = 7.4 Hz), 1.93-1.85 (m, 4 H), 1.36-1.30 (m, 2 H), 1.30-1.23 (m, 4 H); ^{13}C-NMR (75.46 MHz, DMSO-d_6) δ 148.3, 145.1, 144.9, 124.0, 60.2, 30.4, 27.7, 25.1. Anal. ($C_{19}H_{26}Br_2N_4O_2$) C, H, N.

1,8-Octylene-bis-*N,N'*-4-Pyridiniumaldoxime Dibromide (1g)
Yield: 74% as white needles; ^{1}H-NMR (300 MHz, DMSO-d_6) δ 12.83 (s, 2 H), 9.04 (d, 4 H, *J* = 6.4 Hz), 8.43 (s, 2 H), 8.23 (d, 4 H, *J* = 6.6 Hz), 4.55 (t, 4 H, *J* = 7.3 Hz), 1.93-1.85 (m, 4 H), 1.32-1.23 (m, 8 H); ^{13}C-NMR (75.46 MHz, DMSO-d_6) δ 148.3, 145.1, 144.9, 124.0, 60.1, 30.5, 28.1, 25.2. Anal. ($C_{20}H_{28}Br_2N_4O_2$) C, H, N.

1,9-Nonylene-bis-*N,N'*-4-Pyridiniumaldoxime Dibromide (1h)
Yield: 74% as white needles; ^{1}H-NMR (300 MHz, DMSO-d_6) δ 12.83 (s, 2 H), 9.03 (d, 4 H, *J* = 6.5 Hz), 8.43 (s, 2 H), 8.23 (d, 4 H, *J* = 6.7 Hz), 4.55 (t, 4 H, *J* = 7.4 Hz), 1.93-1.85 (m, 4 H), 1.30-1.22 (m, 10 H); ^{13}C-NMR (75.46 MHz, DMSO-d_6) δ 148.3, 145.1, 144.9, 124.0, 60.2, 30.5, 28.5, 28.2, 25.3. Anal. ($C_{21}H_{30}Br_2N_4O_2$) C, H, N.

1,6-Hexylene-bis-*N,N'*-3-Pyridiniumaldoxime Dibromide (2e)
Yield: 82% as white powder; ^{1}H-NMR (300 MHz, DMSO-d_6) δ 12.24 (s, 2 H), 9.32 (s, 2 H), 9.15 (d, 2 H, *J* = 5.7 Hz), 8.73 (d, 2 H, *J* = 8.2 Hz), 8.36 (s, 2 H), 8.18 (dd, 2 H, *J* = 8.0, 6.1 Hz), 4.64 (t, 4 H, *J* = 7.5 Hz), 2.00-1.90 (m, 4 H), 1.40-1.33 (m, 4 H); ^{13}C-NMR (75.46 MHz, DMSO-d_6) δ 144.4, 143.2, 142.5, 141.2, 133.4, 128.0, 60.7, 30.1, 24.6. Anal. ($C_{18}H_{24}Br_2N_4O_2$) C, H, N.

1,7-Heptylene-bis-*N,N'*-3-Pyridiniumaldoxime Dibromide (2f)
Yield: 82% as white powder; ^{1}H-NMR (300 MHz, DMSO-d_6) δ 12.25 (s, 2 H), 9.33 (s, 2 H), 9.11 (d, 2 H, *J* = 6.0 Hz), 8.74 (d, 2 H, *J* = 8.2 Hz), 8.36 (s, 2 H), 8.18 (dd, 2 H, *J* = 8.0, 6.2 Hz), 4.64 (t, 4 H, *J* = 7.4 Hz), 1.99-1.89 (m, 4 H), 1.40-1.25 (m, 6 H); ^{13}C-NMR (75.46 MHz, DMSO-d_6) δ 144.4, 143.2, 142.5, 141.2, 133.4, 128.0, 60.8, 30.4, 27.6, 25.0. Anal. ($C_{19}H_{26}Br_2N_4O_2$) C, H, N.

1,8-Octylene-bis-*N,N'*-3-Pyridiniumaldoxime Dibromide (2g)
Yield: 80% as white powder; ^{1}H-NMR (300 MHz, DMSO-d_6) δ 12.24 (s, 2 H), 9.31 (s, 2 H), 9.09 (d, 2 H, *J* = 6.0 Hz), 8.73 (d, 2 H, *J* = 8.1 Hz), 8.36 (s, 2 H), 8.17 (dd, 2 H, *J* = 8.1, 6.1 Hz), 4.63 (t, 4 H, *J* = 7.5 Hz), 1.96-1.88 (m, 4 H), 1.34-1.25 (m, 8 H); ^{13}C-NMR (75.46 MHz, DMSO-d_6) δ 144.4, 143.2, 142.5, 141.3, 133.4, 128.0, 60.9, 30.5, 28.1, 25.2. Anal. ($C_{20}H_{28}Br_2N_4O_2 \cdot 0.5\ H_2O$) C, H, N.

1,9-Nonylene-bis-*N,N'*-3-Pyridiniumaldoxime Dibromide (2h)
Yield: 70% as white powder; ^{1}H-NMR (300 MHz, DMSO-d_6) δ 12.24 (s, 2 H), 9.31 (s, 2 H), 9.08 (d, 2 H, *J* = 6.1 Hz), 8.73 (d, 2 H, *J* = 8.2 Hz), 8.35 (s, 2 H), 8.17 (dd, 2 H, *J* = 8.1, 6.1 Hz), 4.63 (t, 4 H, *J* = 7.5 Hz), 1.96-1.88 (m, 4 H), 1.32-1.23 (m, 10 H); ^{13}C-NMR (75.46 MHz, DMSO-d_6) δ 144.4, 143.2, 142.5, 141.2, 133.4, 128.0, 60.9, 30.5, 28.4, 28.2, 25.3. Anal. ($C_{20}H_{28}Br_2N_4O_2$) C, H, N.

The general procedure for synthesis of **3b–h** was as follows: 2-Pyridinealdoxime (8.06 g, 66.0 mmol, 2.2 eq.) was added to a solution of 1,7-heptanediol bistriflate (11.88 g, 30.0 mmol) in CH_3CN (90 ml) with stirring at room temperature. After stirring for 3 hr under nitrogen, CH_3CN was removed by using a rotavapor under low pressure. The resulting oily residue was dissolved in water (100 ml) and slowly passed through a column of Dowex 1× 8-200 chloride ion exchange resin (100 g). The elute was concentrated by using a rotavapor under low pressure, further dried under high vacuum, and the resulting crude product was triturated with EtOH/MTBE (30 ml/90 ml) to afford the desired product, **3f** containing 7% of 2-pyridinealdoxime. Further purification by recrystallization from MeOH/MTBE (270 ml/270 ml) gave pure **3f** (9.41 g, 76%) as a white solid.

1,3-Propylene-bis-*N,N'*-2-Pyridiniumaldoxime Dichloride (3b)
Yield: 73% as white powder; ^{1}H-NMR (300 MHz, DMSO-d_6) δ 13.33 (s, 2 H), 9.18 (d, 2 H, *J* = 5.4 Hz), 8.91 (s, 2 H), 8.56 (m, 2 H), 8.43 (d, 2 H, *J* = 7.7 Hz), 8.13 (m, 2 H), 4.90 (t, 4 H, *J* = 7.5 Hz), 2.96 (m, 2 H); ^{13}C-NMR (75.46 MHz, D_2O) δ 146.7, 146.4, 146.1, 142.4, 128.35, 128.31, 55.5, 30.8. Anal. ($C_{15}H_{18}Cl_2N_4O_2$) C, H, N.

1,4-Butylene-bis-*N,N'*-2-Pyridiniumaldoxime Dichloride (3c)
Yield: 80% as white powder; ^{1}H-NMR (300 MHz, DMSO-d_6) δ 13.24 (s, 2 H), 8.98 (d, 2 H, *J* = 5.7 Hz), 8.80 (s, 2 H), 8.55 (m, 2 H), 8.43 (d, 2 H, *J* = 8.1 Hz), 8.09 (m, 2 H), 4.76 (m, 4 H), 1.90 (m, 4 H); ^{13}C-NMR (75.46 MHz, D_2O) δ 149.1, 148.3, 148.2, 144.5, 130.5, 129.9, 60.4, 29.1. Anal. ($C_{16}H_{20}Cl_2N_4O_2 \cdot 2H_2O$) C, H, N.

1,5-Pentylene-bis-*N,N'*-2-Pyridiniumaldoxime Dichloride (3d)
Yield: 77% as white powder; ^{1}H-NMR (300 MHz, DMSO-d_6): δ 13.17 (s, 2 H), 8.99 (d, 2 H, *J* = 6.1 Hz), 8.77 (s, 2 H), 8.56 (m, 2 H), 8.42 (d, 2 H, *J* = 8.1 Hz), 8.11 (m, 2 H), 4.70 (t, 4 H, *J* = 7.4 Hz), 1.85 (m, 4 H), 1.40 (m, 2 H); ^{13}C-NMR (75.46 MHz, D_2O): δ 146.7, 145.7, 142.17,

142.15, 128.1, 127.3, 58.6, 29.6, 22.3; Anal. ($C_{17}H_{22}Cl_2N_4O_2 \cdot 2.5H_2O$) C, H, N.

1,6-Hexylene-bis-*N,N'*-2-Pyridiniumaldoxime Dichloride (3e)
Yield: 85% as white powder; ^{1}H-NMR (300 MHz, DMSO-d_6) δ 13.20 (s, 2 H), 9.05 (d, 2 H, J = 6.0 Hz), 8.79 (s, 2 H), 8.57-8.52 (m, 2 H), 8.40 (d, 2 H, J = 7.8 Hz), 8.12-8.07 (m, 2 H), 4.72 (t, 4 H, J = 7.5 Hz), 1.82-1.75 (m, 4 H), 1.38-1.34 (m, 4 H); ^{13}C-NMR (75.46 MHz, DMSO-d_6) δ 147.0, 146.0, 145.0, 141.2, 127.1, 125.7, 57.5, 29.9, 24.6; Anal. ($C_{17}H_{22}Cl_2N_4O_2 \cdot 2.2H_2O$) C, H, N.

1,7-Heptylene-bis-*N,N'*-2-Pyridiniumaldoxime Dichloride (3f)
Yield: 76% as white powder; ^{1}H-NMR (300 MHz, DMSO-d_6) δ 13.23 (s, 2 H), 9.07 (d, 2 H, J = 6.2 Hz), 8.78 (s, 2 H), 8.57-8.53 (m, 2 H), 8.40 (d, 2 H, J = 8.0 Hz), 8.12-8.07 (m, 2 H), 4.73 (t, 4 H, J = 7.6 Hz), 1.82-1.74 (m, 4 H), 1.36-1.26 (m, 6 H); ^{13}C-NMR (75.46 MHz, DMSO-d_6) δ 146.8, 146.0, 145.1, 141.2, 127.3, 125.9, 57.7, 30.2, 27.7, 25.0; Anal. ($C_{19}H_{26}Cl_2N_4O_2 \cdot 2.6H_2O$) C, H, N.

1,8-Octylene-bis-*N,N'*-2-Pyridiniumaldoxime Dichloride (3g)
Yield: 72% as white powder; ^{1}H-NMR (300 MHz, DMSO-d_6) δ 13.20 (s, 2 H), 9.05 (d, 2 H, J = 6.2 Hz), 8.78 (d, 2 H, J = 1.8 Hz), 8.56-8.51 (m, 2 H), 8.40 (d, 2 H, J = 8.1 Hz), 8.11-8.06 (m, 2 H), 4.72 (t, 4 H, J = 7.6 Hz), 1.71-1.63 (m, 4 H), 1.34-1.23 (m, 8 H); ^{13}C-NMR (75.46 MHz, DMSO-d_6) δ 146.8, 146.1, 145.2, 141.2, 127.3, 125.8, 57.7, 30.2, 28.0, 25.1. Anal. ($C_{20}H_{28}Cl_2N_4O_2 \cdot 0.7H_2O$) C, H, N.

1,9-Nonylene-bis-*N,N'*-2-Pyridiniumaldoxime Dichloride (3h)
Yield: 75% as white powder; ^{1}H-NMR (300 MHz, DMSO-d_6) δ 13.19 (s, 2 H), 9.03 (d, 2 H, J = 6.9 Hz), 8.79 (s, 2 H), 8.56-8.53 (m, 2 H), 8.40 (d, 2 H, J = 8.0 Hz), 8.12-8.06 (m, 2 H), 4.71 (t, 4 H, J = 7.6 Hz), 1.82-1.74 (m, 4 H), 1.34-1.21 (m, 10 H); ^{13}C-NMR (75.46 MHz, DMSO-d_6) δ 146.8, 146.1, 145.1, 141.2, 127.3, 125.8, 57.7, 30.3, 28.4, 28.2, 25.2. Anal. ($C_{17}H_{22}Cl_2N_4O_2 \cdot 1.3H_2O$) C, H, N.

Biological Testing

A reactivation assay used freshly inhibited hAChE in membranes prepared from human red blood cells. A suspension of washed red cell membranes (500 μl aliquots of a 50-fold dilution) were treated for 60 min at 23°C with organophosphate anticholinesterase (echothiophate or, in particular experiments, isoflurophate), 10^{-7} M in 50 mM Tris HCl (pH 7.4). Subsequently, the hAChE inhibitor was removed by two successive rinses involving centrifugation (8000 × g, 10 min) and resuspension in the original volume of buffer. This treatment regularly led to a stable 99% inhibition of hAChE (control experiments with the reversible anticholinesterase, BW284C51, showed that the rinsing was adequate to remove free inhibitor). Spontaneous reactivation was negligible over periods of up to 2 hr in the absence of reactivator (<2%). Reactivating agents were added at a range of concentrations for up to 1 hr at 37°C. Following the reactivation step, red cell membranes were rinsed again (see above), and 10 μl aliquots were transferred to a microtiter plate for assay by a standard spectrophotometric method [40]. Reagents were added to wells of a microtiter plate in this order: hAChE extract, reaction buffer, substrate-free reaction cocktail, and bis-oxime. After a 5 min preincubation, acetylthiocholine iodide substrate was added at final concentrations from 0.033 mM to 1 mM, and the reactions were monitored in a plate reader.

Analysis of enzyme reactivation assumed that the tested oximes bound rapidly and reversibly to phosphorylated enzyme, slowly accepted the phosphate residue, then rapidly dissociated, according to Scheme I of Figure 2. For analytical simplicity, the second reaction was treated as irreversible, since back reaction is negligible at the low expected concentrations of phosphorylated oxime. Thus, the reactivation of phosphorylated hAChE was described by Equation 1:

$$R = E(1 - e^{-k_3(\frac{D}{D+K_D})t}). \quad (1)$$

Here, R is recovered enzyme activity, E is total activity before inhibition, t is time in minutes, k_3 is the rate constant for reactivation, D is oxime concentration, and K_D is the dissociation constant of the reversible complex between oxime and phosphorylated hAChE. To solve for the parameters, reactivation data were fitted to Equation 1 by nonlinear regression with SigmaPlot 5.01 (Jandel Scientific). This analysis neglects the competing dealkylation shown in Scheme I of Figure 2 and thus results in about 30% loss of the reactivation in the case of isoflurophate, which has appreciable dealkylation under the test condition.

In order to estimate the dissociation constant of the oxime complex with *unphosphorylated* hAChE, we used the inhibitory properties of our compounds to determine K_i values. For this purpose, hAChE activity was measured at multiple substrate concentrations in the presence of multiple concentrations of oxime. Maximal velocities at each concentration of oxime were calculated by fitting data to the standard Michaelis-Menten equation. Because double reciprocal plots of these data all intersected on or near the x axis, the inhibition was treated as noncompetitive. Accordingly, the inhibition constants were derived by fitting to Equation 2:

$$V_{max\ app} = V_{max}/(1 + D/K_i). \quad (2)$$

Here, $V_{max\ app}$ is apparent maximal velocity in the presence of oxime, V_{max} is the true maximal velocity, D is oxime concentration, and K_i is the inhibition constant.

DFT Calculations

Four different conformations of 2-PAM were generated manually with the QUANTA program [41]. The structures optimized with the CHARMm force field [42] were subject to energy minimizations and frequency calculations with the B3LYP/6-31+G(d,p) method using the Gaussian 98 program [43–45]. The structures optimized in vacuo were subjected to energy minimizations and frequency calculations using the B3LYP/6-31+G(d,p) method in water (ε = 78.39) with the Onsager solvent model [19–22]. No imaginary frequency was found for any of the optimized structures reported in Figure 1.

Molecular Mechanics Calculations

The 3D structures of diisopropylphosphoryl-hAChE, 2-PAM, 4-PAM, **1b** and **3f** were generated by employing the PREP, LINK, EDIT, PARM, and SANDER modules of the AMBER 5.0 program [46] with the force field by Cornell et al. (parm99.dat) [47] and additional force field parameters provided in the Supplemental Data. The RESP charges of these molecules were generated by calculating electrostatic potentials using the GAUSSIAN 98 program [43] with the HF/6-31G*//HF/6-31G* method followed by a two-stage fitting using the RESP module of the AMBER 5.0 program [48]. The RESP charges are available in the Supplemental Data. The diisopropylphosphoryl-hAChE structure was generated from the amino acid sequence of hAChE (Entrez Protein Database 1B41A; http://www.ncbi.nlm.nih.gov) and the coordinates of corresponding residues in the X-ray structure of hAChE (PDB ID code 1B41) [49]. Modifications included (1) replacement of Ser200 with a diisopropylphosphorylated serine residue (the residue file is available in the Supplemental Data); (2) protonation or deprotonation of the Arg, Lys, Asp, Glu, His, and Cys residues; (3) conformational search of the diisopropylphosphoryl group in the active site of hAChE (vide infra); (4) adjustment of the acyl pocket loop conformation according to the conformation found in the X-ray structure of an aged phosphylated hAChE (PDB ID code 2DFP) [32]; (5) energy minimization of the resulting structure; and (6) refinement of the energy-minimized structure by 20 independent 1.0 ns (1.0 fs time step) MD simulations with different initial velocities (vide infra). The protonation states of the Arg, Lys, Asp, Glu, His, and Cys residues were determined according to the published protocol [50]. His440 residue that constitutes the catalytic triad was treated as protonated because Ser200 was diisopropylphosphorylated.

Conformational Analyses

Conformational searches were performed for the diisopropylphosphoryl group, **1b** and **3f**, employing the CONSER program (devised by Y.-P. Pang). This program first generated conformations by specifying all discrete possibilities at 120° of arc increments in a range of 0 to 360 for all rotatable bonds of the diisopropylphosphoryl group, **1b** and **3f**. It then optimized such conformers with the RESP charges and the Cornell et al. force field (parm99.dat) [47]. Afterwards, it performed a cluster analysis to delete duplicates. These duplicates include those caused by C2 symmetry of the 4-pyridiniumaldoxime

ring. In the cluster analysis, two conformers were judged different if at least one of the defined torsions differed by more than 30̊ of arc.

Docking Studies

All docking studies were performed by using the EUDOC program (ceramic version) according to the published procedure [50]. This program systematically translates and rotates a ligand in a putative binding pocket of a receptor to search for energetically favorable orientations and positions of the ligand. The translational and rotational increments in these docking studies were set at 1.0 Å and 10° of arc, respectively. All conformations of pyridiniumaldoximes were used in the docking studies. The intermolecular interaction energies were calculated without nonbonded distance cut-off. The dielectric constant used in the calculation of intermolecular interaction energy was set to 1.0.

MD Simulations

The MD simulations employed the SANDER module of the AMBER 7.0 program [46] with the Cornell et al. force field (parm99.dat) [47] and additional force field parameters provided in the Supplemental Data. These simulations used (1) a dielectric constant of 1.0; (2) the Berendsen coupling algorithm [51]; (3) a periodic boundary condition in the NPT ensemble at constant temperature of 300 K and constant pressure of 1 atm with isotropic molecule-based scaling; (4) the Particle Mesh Ewald (PME) method to calculate the long-range electrostatic interactions [52]; and (5) default values of all other inputs of the SANDER module. By employing the EDIT module, the hAChE or its complex structure was solvated with about 15,000 TIP3P water molecules [53] (EDIT input: NCUBE = 20, QH = 0.4170, DISO = 2.20, DISH = 2.00, CUTX = 8.2, CUTY = 8.2, and CUTZ = 8.2), including 26 crystallographically determined water molecules bound inside the protein. The resulting systems (circa 52,000 atoms) were first energy minimized for 500 steps to remove close van der Waals contacts in the system, and then slowly heated to 300 K (10 K/ps) and equilibrated for 500 ps before a 500 ps simulation. Among the 10 or 20 protein conformations simulated with different initial velocities, the most energetically stable conformation was obtained by averaging the potential energies of hAChE or its complex in water in each simulation followed by cooling the last trajectory of the simulation with the lowest average potential energy to 0 K (3 K/ps). All water molecules that are 1.85 Å or more away from the protein complex were not included in the calculation of intermolecular interaction energies.

Supplemental Data

Elemental analysis results and force field parameters for oxime derivatives and diisopropylphosphorylated serine are available at http://www.chembiol.com/cgi/content/full/10/6/491/DC1.

Acknowledgments

Support by the Mayo Foundation, the NIH (NS29646 to W.S.B.), the Defense Advanced Research Projects Agency (DAAD19-01-1-0322 to Y.-P.P.), the High Performance Computing Modernization Program of the DOD (allocations from ASC, AHPCRC, and ERDC to Y.-P.P.), and the University of Minnesota Supercomputing Institute (Y.-P.P.).

Received: December 25, 2002
Revised: March 30, 2003
Accepted: April 4, 2003
Published: June 20, 2003

References

1. Taylor, P. (1996). Anticholinesterase Agents. In Goodman & Gilman's The Pharmacological Basis of Therapeutics, J.G. Hardman, A.G. Gilman, and L.E. Limbird, eds. (New York: McGraw-Hill), pp. 161–197.
2. Wilson, I.B., and Ginsburg, S. (1955). A powerful reactivator of alkylphosphate-inhibited acetylcholinesterase. Biochim. Biophys. Acta *18*, 168–170.
3. Wilson, I.B., and Ginsburg, S. (1958). Reactivation of alkylphosphate inhibited acetylcholinesterase by bis quaternary derivatives of 2-pam and 4-pam. Biochem. Pharmacol. *1*, 200–206.
4. Fleisher, J.H., Harris, L.W., and Murtha, E.F. (1967). Reactivation by pyridinium aldoxime methochloride (PAM) of inhibited cholinesterase activity in dogs after poisoning with pinacolyl methylphosphonofluoridate (soman). J. Pharmacol. Exp. Ther. *156*, 345–351.
5. Saxena, A., Viragh, C., Frazier, D.S., Kovach, I.M., Maxwell, D.M., Lockridge, O., and Doctor, B.P. (1998). The ph dependence of dealkylation in soman-inhibited cholinesterases and their mutants - further evidence for a push-pull mechanism. Biochemistry *37*, 15086–15096.
6. Viragh, C., Kovach, I.M., and Pannell, L. (1999). Small molecular products of dealkylation in soman-inhibited electric eel acetylcholinesterase. Biochemistry *38*, 9557–9561.
7. Hallek, M., and Szinicz, L. (1988). Effects of some mono- and bisquaternary ammonium compounds on the reactivatability of soman-inhibited human acetylcholinesterase in vitro. Biochem. Pharmacol. *37*, 819–825.
8. Boskovi, B. (1981). The treatment of Soman poisoning and its perspectives. Fundam. Appl. Toxicol. *1*, 203–213.
9. Poziomek, E.J., Hackley, J.B.E., and Steinberg, G.M. (1958). Pyridinium aldoximes. J. Org. Chem. *23*, 714–717.
10. Patocka, J., and Bielavsky, J. (1972). Affinity of bis-quaternary pyridinedialdoximes for the active centre of intact and isopropylmethylphosphonylated acetylcholinesterase. Collection. Czechoslov. Chem. Commun. *37*, 2110–2117.
11. Hobbiger, F., O'Sullivan, D.G., and Sadler, P.W. (1958). New potent reactivators of acetylcholinesterase inhibited by tetraethyl pyrophosphate. Nature *182*, 1498–1499.
12. Hobbiger, F., and Sadler, P.W. (1958). Protection by oximes of bis-pyridinium ions against lethal diisopropyl phosphonofluoridate poisoning. Nature *182*, 1672–1673.
13. Hobbiger, F., and Sadler, P.W. (1959). Protection against lethal organophosphate poisoning by quaternary pyridine aldoximes. Br. J. Pharmacol. *14*, 192–201.
14. Berry, W.K., Davies, D.R., and Green, A.L. (1959). Oximes of $\alpha\omega$-diquaternary alkane salts as antidotes to organophosphate anticholinesterases. Br. J. Pharmacol. *14*, 186–191.
15. Ginsburg, S., and Wilson, I.B. (1957). Oximes of the pyridine series. J. Am. Chem. Soc. *79*, 481–485.
16. Wilson, I.B., Ginsburg, S., and Quan, C. (1958). Molecular complementariness as basis for reactivation of alkyl phosphate-inhibited enzyme. Arch. Biochem. *77*, 286–296.
17. Crepaux, D., and Lehn, J.-M. (1975). Application des mesures de couplages 15N-H a la determination de configuration d'oximes. Org. Magn. Reson. *7*, 524–526.
18. Jahng, Y., Park, J.G., Yoo, J.W., Kim, S.Y., Kim, T., and Yang, J.H. (2000). Synthesis and biological activity of conformationally controlled 2-PAM derivatives. Arch. Pharm. Res. *23*, 222–225.
19. Wong, M.W., Frisch, M.J., and Wiberg, K.B. (1991). Solvent effects 1. The mediation of electrostatic effects by solvents. J. Am. Chem. Soc. *113*, 4776–4782.
20. Wong, M.W., Wiberg, K.B., and Frisch, M.J. (1992). Solvent effects 2. Medium effect on the structure, energy, charge density, and vibrational frequencies of sulfamic acid. J. Am. Chem. Soc. *114*, 523–529.
21. Wong, M.W., Wiberg, K.B., and Frisch, M.J. (1991). SCF second derivatives and electric field properties in a reaction field. J. Chem. Phys. *95*, 8991–8998.
22. Wong, M.W., Wiberg, K.B., and Frisch, M.J. (1992). Solvent effects 3. Tautomeric equilibria of formamide and 2-pyridone in the gas phase and solution: an ab initio SCRF study. J. Am. Chem. Soc. *114*, 1645–1652.
23. Caristrom, D. (1966). Crystallographic study of N-methyl-pyridine-2-aldoxime (2-PAM) halides. Acta Chem. Scand. *20*, 1240–1246.
24. Pang, Y.P., Quiram, P., Jelacic, T., Hong, F., and Brimijoin, S. (1996). Highly potent, selective, and low cost bis-tetrahydroaminacrine inhibitors of acetylcholinesterase. Steps toward novel drugs for treating Alzheimer's disease. J. Biol. Chem. *271*, 23646–23649.
25. Barak, D., Kronman, C., Ordentlich, A., Ariel, N., Bromberg, A., Marcus, D., Lazar, A., Velan, B., and Shafferman, A. (1994).

Acetylcholinesterase peripheral anionic site degeneracy conferred by amino acid arrays sharing a common core. J. Biol. Chem. *269*, 6296–6305.
26. Salomon, M.F., and Salomon, R.G. (1979). The peroxide transfer reaction. J. Am. Chem. Soc. *101*, 4290–4299.
27. Bedford, C.D., Harris, R.N., III, Howd, R.A., Goff, D.A., Koolpe, G.A., Petesch, M., Koplovitz, I., Sultan, W.E., and Musallam, H.A. (1989). Quaternary salts of 2-[(hydroxyimino)methyl]imidazole. 3. Synthesis and evaluation of (alkenyloxy)-, (alkynyloxy)-, and (aralkyloxy)methyl quaternarized 2-[(hydroxyimino)methyl]-1-alkylimidazolium halides as reactivators and therapy for soman intoxication. J. Med. Chem. *32*, 504–516.
28. Caves, L.S.D., Evanseck, J.D., and Karplus, M. (1998). Locally accessible conformations of proteins - multiple molecular dynamics simulations of crambin. Protein Sci. *7*, 649–666.
29. Smith, L.J., Daura, X., and van Gunsteren, W.F. (2002). Assessing equilibration and convergence in biomolecular simulations. Proteins *48*, 487–496.
30. Snow, C.D., Nguyen, N., Pande, V.S., and Gruebele, M. (2002). Absolute comparison of simulated and experimental protein-folding dynamics. Nature *420*, 102–106.
31. Zagrovic, B., Snow, C.D., Shirts, M.R., and Pande, V.S. (2002). Simulation of folding of a small alpha-helical protein in atomistic detail using worldwide-distributed computing. J. Mol. Biol. *323*, 927–937.
32. Millard, C.B., Kryger, G., Ordentlich, A., Greenblatt, H.M., Harel, M., Raves, M.L., Segall, Y., Barak, D., Shafferman, A., Silman, I., et al. (1999). Crystal structures of aged phosphonylated acetylcholinesterase: Nerve agent reaction products at the atomic level. Biochemistry *38*, 7032–7039.
33. Millard, C.B., Koellner, G., Ordentlich, A., Shafferman, A., Silman, I., and Sussman, J.L. (1999). Reaction products of acetylcholinesterase and VX reveal a mobile histidine in the catalytic triad. J. Am. Chem. Soc. *121*, 9883–9884.
34. Levitt, M., and Perutz, M.F. (1988). Aromatic rings act as hydrogen bond acceptors. J. Mol. Biol. *201*, 751–754.
35. Bernstein, F.C., Koetzle, T.F., Williams, G.J., Meyer, E.E., Jr., Brice, M.D., Rodgers, J.R., Kennard, O., Shimanouchi, T., and Tasumi, M. (1977). The Protein Data Bank: a computer-based archival file for macromolecular structures. J. Mol. Biol. *112*, 535–542.
36. Berman, H.M., Westbrook, J., Feng, Z., Gilliland, G., Bhat, T.N., Weissig, H., Shindyalov, I.N., and Bourne, P.E. (2000). The Protein Data Bank. Nucleic Acids Res. *28*, 235–242.
37. Leader, H., Vincze, A., Manisterski, B., Rothschild, N., Dosoretz, C., and Ashani, Y. (1999). Characterization of O,O-diethylphosphoryl oximes as inhibitors of cholinesterases and substrates of phosphotriesterases. Biochem. Pharmacol. *58*, 503–515.
38. Wong, D.M., Greenblatt, H.M., Dvir, H., Carlier, P.R., Han, Y.F., Pang, Y.P., Silman, I., and Sussman, J.L. (2003). Acetylcholinesterase complexed with bivalent ligands related to huperzine A: Experimental evidence for species-dependent protein-ligand complementarity. J. Am. Chem. Soc. *125*, 363–373.
39. Bar-On, P., Millard, C.B., Harel, M., Dvir, H., Enz, A., Sussman, J.L., and Silman, I. (2002). Kinetic and structural studies on the interaction of cholinesterases with the anti-Alzheimer drug rivastigmine. Biochemistry *41*, 3555–3564.
40. Ellman, G.L., Courtney, K.D., Andres, V.J., and Featherstone, R.M. (1961). A new and rapid colorimetric determination of acetylcholinesterase activity. Biochem. Pharmacol. *7*, 88–95.
41. QUANTA/CHARMm. (1997). Molecular Simulations Inc. San Diego, CA.
42. Brooks, B.R., Bruccoleri, R.E., Olafson, B.D., States, D.J., Swaminathan, S., and Karplus, M. (1983). A program for macromolecular energy, minimization, and dynamics calculations. J. Comput. Chem. *4*, 187–217.
43. Frisch, M.J., Trucks, G.W., Schlegel, H.B., Gill, P.M.W., Hohnson, B.G., Robb, M.A., Raghavachari, K., Al-Laham, M.A., Zakrzewski, V.G., Ortiz, J.V., et al. (1999). GAUSSIAN *98*, Revision A.7. Gaussian, Inc. Pittsburgh, PA.
44. Becke, A.D. (1993). Density-functional thermochemistry: 3. The role of exact exchange. J. Chem. Phys. *98*, 5648–5652.
45. Lee, C., Yang, W., and Parr, R.G. (1988). Development of the Colle-Salvetti correlation-energy formula into a functional of the electron density. Phys. Rev. B Condens. Matter *37*, 785–789.
46. Pearlman, D.A., Case, D.A., Caldwell, J.W., Ross, W.S., Cheatham, T.E., III, Debolt, S., Ferguson, D., Seibel, G., and Kollman, P.A. (1995). AMBER, a package of computer programs for applying molecular mechanics, normal mode analysis, molecular dynamics and free energy calculations to simulate the structural and energetic properties of molecules. Comput. Phys. Commun. *91*, 1–41.
47. Cornell, W.D., Cieplak, P., Bayly, C.I., Gould, I.R., Merz, K.M., Jr., Ferguson, D.M., Spellmeyer, D.C., Fox, T., Caldwell, J.W., and Kollman, P.A. (1995). A second generation force field for the simulation of proteins, nucleic acids, and organic molecules. J. Am. Chem. Soc. *117*, 5179–5197.
48. Cieplak, P., Cornell, W.D., Bayly, C., and Kollman, P.A. (1995). Application of the multimolecule and multiconformational resp methodology to biopolymers: charge derivation for DNA, RNA, and proteins. J. Comput. Chem. *16*, 1357–1377.
49. Kryger, G., Harel, M., Giles, K., Toker, L., Velan, B., Lazar, A., Kronman, C., Barak, D., Ariel, N., Shafferman, A., et al. (2000). Structures of recombinant native and E202Q mutant human acetylcholinesterase complexed with the snake-venom toxin fasciculin-II. Acta Crystallogr. D Biol. Crystallogr. *56*, 1385–1394.
50. Pang, Y.P., Perola, E., Xu, K., and Prendergast, F.G. (2001). EUDOC: A computer program for identification of drug interaction sites in macromolecules and drug leads from chemical databases. J. Comput. Chem. *22*, 1750–1771.
51. Berendsen, H.J.C., Postma, J.P.M., van Gunsteren, W.F., Di Nola, A., and Haak, J.R. (1984). Molecular dynamics with coupling to an external bath. J. Chem. Phys. *81*, 3684–3690.
52. Darden, T.A., York, D.M., and Pedersen, L.G. (1993). Particle Mesh Ewald: An N log(N) method for Ewald sums in large systems. J. Chem. Phys. *98*, 10089–10092.
53. Jorgensen, W.L., Chandreskhar, J., Madura, J.D., Impey, R.W., and Klein, M.L. (1982). Comparison of simple potential functions for simulating liquid water. J. Chem. Phys. *79*, 926–935.

Accession Numbers

The coordinates of **3f**- and **1b**-diisopropylphosphoryl-*Torpedo*-AChE complexes adopting the loop-in conformation were deposited to the PDB [35, 36] on June 23, 2001 (PDB ID codes 1JGA and 1JGB) and were superseded by the corresponding ones of hAChE adopting the loop-out conformation on March 31, 2003. Residue numbers in the structures deposited to the PDB deviate by one from the residue numbers reported in the Entrez Protein Database (1B41A).